Supporting Information

Quantitative Analysis of the Alignment Degree of GO Nanosheets.

The degree of alignment of the GO nanosheets was quantitatively estimated using an orientation distribution coefficient, *S*, which was defined by Hermans as the mean of the second-order Legendre polynomial (1):

$$S = \left\langle \frac{1}{2}\left(3\cos^2\theta - 1\right) \right\rangle \qquad \text{(S1)}$$

This orientation distribution coefficient can be correlated with the azimuthal dependence of the scattered intensity, *I (θ)*, by

$$\left\langle \cos^2\theta \right\rangle = \frac{\int_0^{\frac{\pi}{2}} I(\theta)\cos^2\theta \sin\theta d\theta}{\int_0^{\frac{\pi}{2}} I(\theta)\sin\theta\, d\theta} \qquad \text{(S2)}$$

A perfect orientation corresponds to $S = 1$, whereas a completely random orientation possesses an *S* value of 0.

Preparation of Liposome Stock Solution.

Liposomes were prepared via the film rehydration method. Briefly, 20 mg of 1, 2-dioleoyl-sn-glycero-3-phosphocholine (DOPC; Avanti Polar Lipids) in chloroform was dried in a glass tube under a stream of nitrogen gas to form a lipid film. The DOPC film was put under vacuum overnight to remove residual chloroform. To form multilamellar vesicles, the dried film was subsequently rehydrated with agitation in 50 mM 3-(N-morpholino)propanesulfonic acid (MOPS) buffer (pH 7.5) with 50 mM of a fluorescent dye [5(6) carbeoxyfluorescein, CF; Acros Organics]. The lipid mixture was then extruded 21 times using a mini-extruder (Avanti Polar Lipids) through a polycarbonate track-etched membrane with 100-nm pore size (GE Healthcare Life Sciences) to form unilamellar vesicles. The lipid vesicle solution was passed through a HiTrap Desalting column (GE Healthcare Life Sciences) equilibrated with 50 mM MOPS and 90 mM NaCl (pH 7.5) to remove the CF fluorescent dye that was not encapsulated by the liposomes. The prepared liposome stock solution had a DOPC concentration of ~4 $mg \cdot mL^{-1}$ and vesicles with a hydrodynamic diameter of 140 nm, as determined by dynamic light scattering (ALV GmbH). A freshly prepared stock solution was used for each day of experiments.

Quantitation of Reactive Oxygen Species (ROS) in GO Suspension.

Generation of the four most important ROS, i.e., singlet oxygen, hydroxyl radical, superoxide radical anion, and hydrogen peroxide, was assessed in a solution of dispersed GO using the respective chemical probes. Solutions containing 200 μg·mL^{-1} GO and individual ROS probe were stored in the dark at room temperature. Aliquots of the solution were taken at various time points for kinetic analysis of ROS generation. Additionally, formation of ROS induced by GO was measured in bacterial suspensions (10^7 cfu·mL^{-1} of *E. coli*).

Singlet Oxygen. The steady-state concentration of $^1O_2$ ($[^1O_2]_{ss}$) was determined using the selective probe furfuryl alcohol (FFA; Sigma-Aldrich) (2) using

$$[^1O_2]_{ss} = \frac{k_{obs}^{FFA}}{k_{rxn}^{FFA}} \qquad \text{(S3)}$$

where k_{obs}^{FFA} the first-order rate constant for FFA degradation, and $k_{rxn}^{FFA} = 1.0 \times 10^8$ M^{-1}·s^{-1} (3).

Solutions containing 200 μg·mL^{-1} GO and 50 μM FFA were stored in the dark at room temperature. Aliquots (100 μL) of the solution were taken to an HPLC vial with glass insert at various time points. The FFA concentration was analyzed using an Agilent high-performance liquid chromatography (HPLC) coupled to a photodiode array detector (PDA; Agilent 1100); 50 μL of each sample was injected. Separation was carried out in a C18 column at 20 °C with an isocratic mobile phase of 80% phosphoric buffer (pH 2.3) and 20% acetonitrile (v/v) at a flow rate of 2 mL·min^{-1}. Quantification of FFA was performed using absorption at 220 nm, where the FFA peak was detected with a retention time of 1.35 min.

Hydroxyl Radical. Potassium terephthalic acid (TPA; Sigma−Aldrich) was used as a probe to determine the cumulative generation of •OH ([•OH]) by the formation of hydroxyterephthalate (hTPA) (4, 5). Solutions containing 200 μg·mL^{-1} GO and 1 mM TPA were stored in the dark at room temperature. Aliquots (100 μL) of the solution were added to an LC vial with glass insert at various time points.

Analysis of hTPA was conducted using an Agilent HPLC coupled to a PDA detector (Agilent 1100); 50 μL of each sample was injected. Separation was carried out in a C18 column at 20 °C with an isocratic mobile phase of 65% phosphoric buffer (pH 2.3) and 35% methanol (v/v) at a

flow rate of 2 mL·min^{-1}. Quantification of hTPA was performed using absorption at 315 nm, where the hTPA peak was detected with a retention time of 3.34 min.

The concentration of hTPA was determined using a calibration curve obtained with hTPA standard. [$^{\bullet}$OH] was determined according to

$$[^{\bullet}OH]_{ss} = \frac{[hTPA]}{0.35} \qquad \text{(S4)}$$

This relation assumes 100% capture of $^{\bullet}$OH by the TPA probe and a yield of 0.35 for hTPA formation upon each reaction of TPA with $^{\bullet}$OH (4).

Superoxide Radical Anion. 2,3-Bis-(2-methoxy-4-nitro-5-sulfophenyl)-2H-tetrazolium-5-carboxanilide (XTT; Sigma−Aldrich) was used as a probe to determine the generation of $O_2^{\bullet-}$. XTT reacts with $O_2^{\bullet-}$ to generate XTT-formazan. Solutions containing 200 μg·mL^{-1} GO and 100 μM XTT were stored in the dark at room temperature Sample (1 mL) was added into a cuvette and the formation of XTT-formazan was determined via absorption at 470 nm using a UV-Vis spectrophotometer (RF-5301PC; Shimadzu).

Hydrogen Peroxide. Ampliflu Red (Sigma−Aldrich) was used to probe H_2O_2 generation by the formation of resorufin in the presence of horseradish peroxidase (6, 7). H_2O_2 standard solution was used to calibrate the resorufin peak area in relation to H_2O_2 concentration. Solutions containing 200 μg·mL^{-1} GO were stored in the dark at room temperature. Aliquots (50 μL) of the solution were removed to an LC vial with glass insert at various time points and mixed with 50 μL solutions containing Ampliflu Red (100 μM) and horseradish peroxidase (0.05 U·mL^{-1}). Quantification of resorufin in the mixture solution was conducted using an Agilent HPLC coupled to a PDA detector; 50 μL of each sample was injected. Separation was carried out in a C18 column at 20 °C with an isocratic mobile phase of 55% sodium citrate buffer (with 10% methanol, pH 7.4) and 45% acetonitrile (v/v) at a flow rate of 2 mL·min^{-1}. Quantification of resorufin was performed using absorption at 560 nm, where the resorufin peak was detected with a retention time of 1.45 min.

References

1. Hermans JJ, Hermans PH, Vermaas D, & Weidinger A (1946) Quantitative evaluation of orientation in cellulose fibres from the X-ray fibre diagram. *Recl Trav Chim Pays-Bas* 65(6):427–447.
2. Burns JM*, et al.* (2012) Methods for reactive oxygen species (ROS) detection in aqueous environments. *Aquat Sci* 74(4):683–734.
3. Appiani E, Ossola R, Latch DE, Erickson PR, & McNeill K (2017) Aqueous singlet oxygen reaction kinetics of furfuryl alcohol: effect of temperature, pH, and salt content. *Env Sci Process Impact* 19(4):507–516.
4. Page SE, Arnold WA, & McNeill K (2010) Terephthalate as a probe for photochemically generated hydroxyl radical. *J Environ Monit* 12(9):1658–1665.
5. Janssen EML, Marron E, & McNeill K (2015) Aquatic photochemical kinetics of benzotriazole and structurally related compounds. *Env Sci Process Impact* 17(5):939–946.
6. Zhou M, Diwu Z, Panchuk-Voloshina N, & Haugland RP (1997) A Stable Nonfluorescent Derivative of Resorufin for the Fluorometric Determination of Trace Hydrogen Peroxide: Applications in Detecting the Activity of Phagocyte NADPH Oxidase and Other Oxidases. *Anal Biochem* 253(2):162–168.
7. Chu C*, et al.* (2016) Photochemical and Nonphotochemical Transformations of Cysteine with Dissolved Organic Matter. *Environ Sci Technol* 50(12):6363–6373.

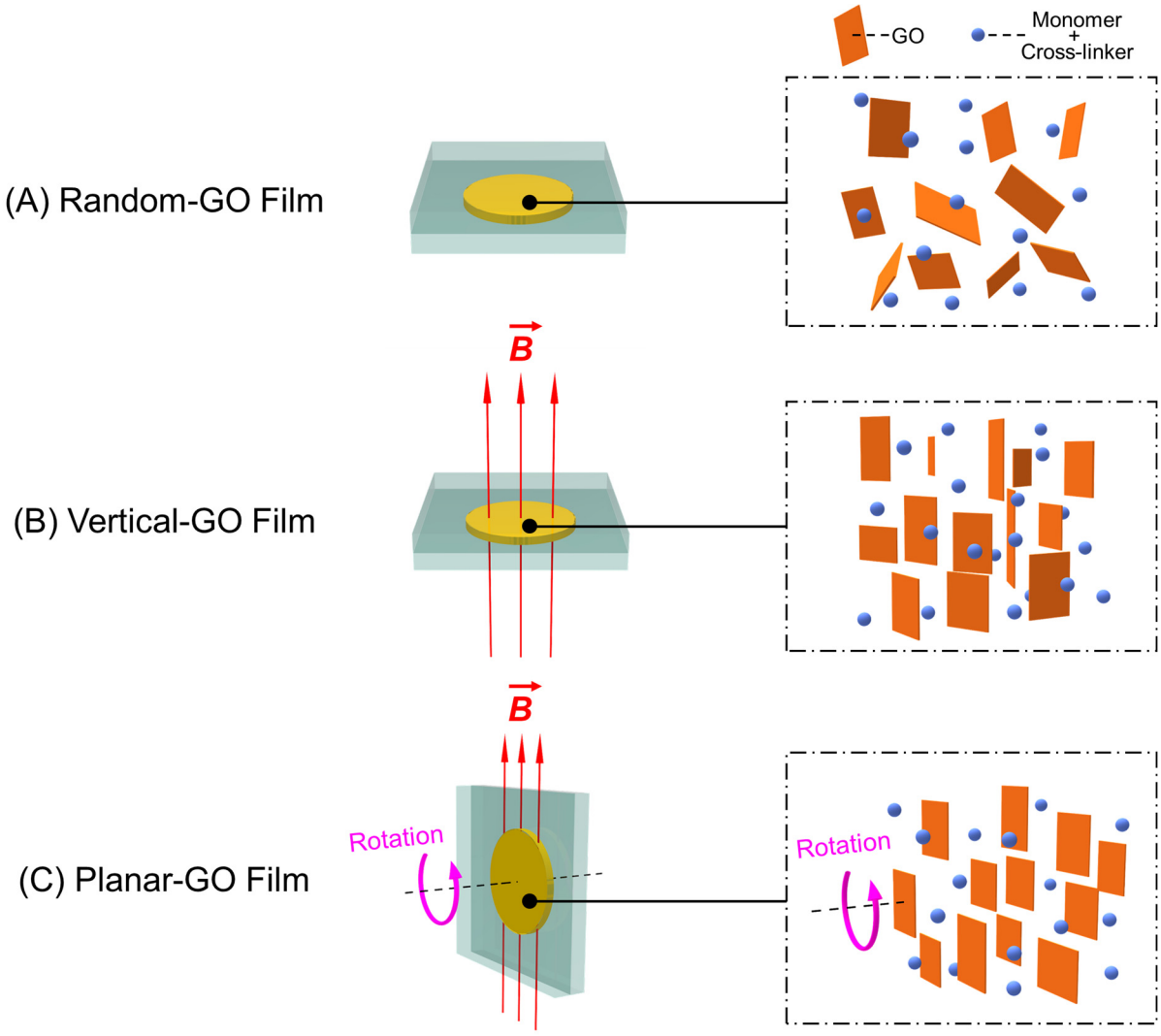

Figure S1. Schematic illustration of the field-alignment methods used to fabricate composite films with different orientations of GO nanosheets exposed on the surface. (A) Random-GO film was fabricated without any field alignment, in which the GO nanosheets were isotropically distributed inside the film. (B) Vertical-GO film was fabricated by applying the magnetic field perpendicular to the glass substrates, in which GO nanosheets aligned in parallel with the field and therefore orthogonally to the film surface (i.e., vertically aligned). (C) Planar-GO film was formed by applying the magnetic field parallel to the glass substrates, which were continuously rotated around an axis perpendicular to the field. In this case, the normal axes of the GO nanosheets uniformly aligned along the rotation axis, which enabled the exposure of planarly aligned GO nanosheets on the film surface.

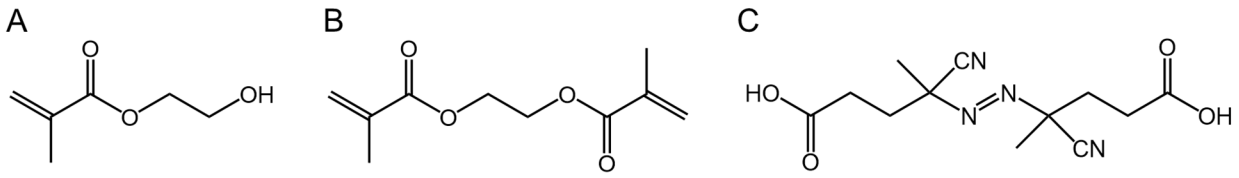

Figure S2. Chemical structures of molecules used to preserve the orientation of the aligned GO nanosheets during fabrication of GO composite films. (A) Monomer: 2-hydroxyethyl methacrylate (HEMA). (B) Cross-linker: ethylene glycol dimethacrylate (EGDMA). (C) Photoinitiator: 4,4′-azobis(4-cyanovaleric acid) (ACVA). GO was dispersed in a HEMA mixture (HEMA/EGDMA/ ACVA = 100:10:0.5 by weight) at a concentration of 2.1 $g \cdot L^{-1}$.

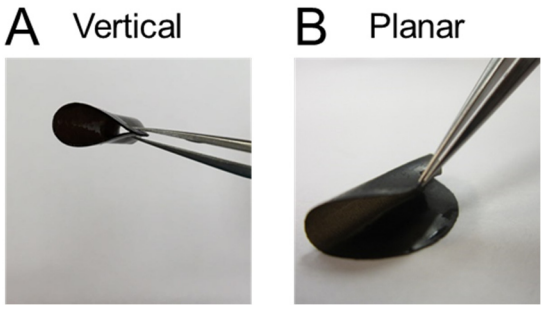

Figure S3. Representative photos of GO composite films with (A) vertical and (B) planar orientations. All the composite films are tough and mechanically coherent with good resistance to water swelling.

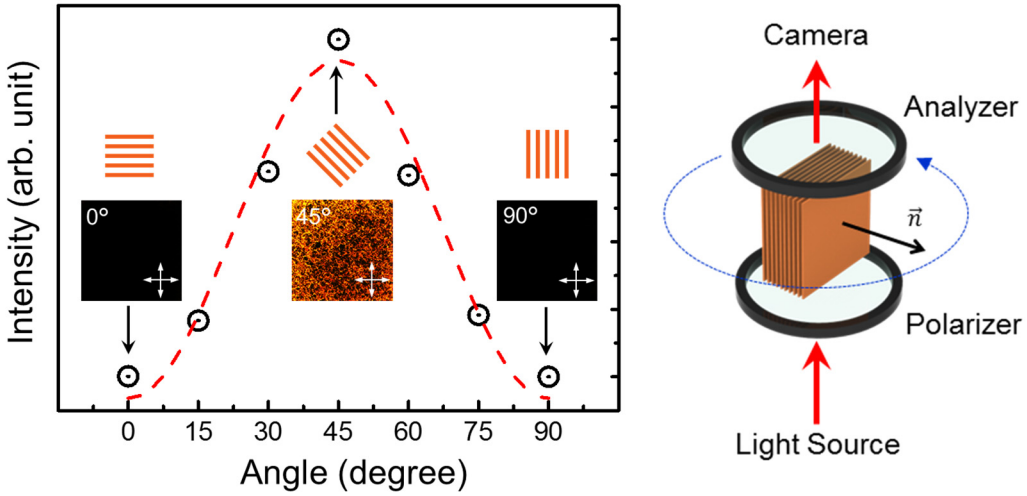

Figure S4. Transmission intensity under polarized optical microscopy of a GO composite film with uniaxial alignment. The sample was positioned such that normal of the uniformly aligned nanosheets, $\vec{n}$, was orthogonal to the direction of light propagation, as illustrated by the schematic at the right. Transmission intensity was recorded as the sample was rotated around the direction of light propagation. The transmission intensity varies with a 90-degree period, which is consistent with the uniform alignment of the normal that is also the optic axis of each GO nanosheet.

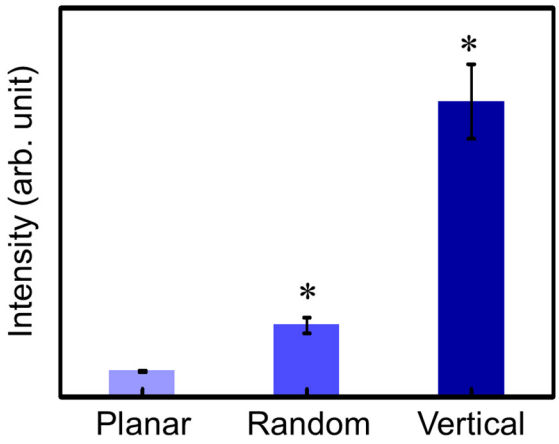

Figure S5. Transmission intensity under polarized optical microscopy (POM) of GO composite films. Normal axes of the film surfaces are along the direction of light propagation. Transmission intensity in POM images of different GO composite films followed the order Vertical > Random > Planar, indicating that the Vertical-GO film possesses more vertically aligned GO nanosheets within the bulk film compared to the Random-GO film and the Planar-GO film. For each film, five measurements were performed on five different samples. Error bars represent the standard deviation of the five measurements. An asterisk (*) indicates statistically significant differences in means compared with Planar film (Student's *t* test, $n = 3$, $P < 0.05$).

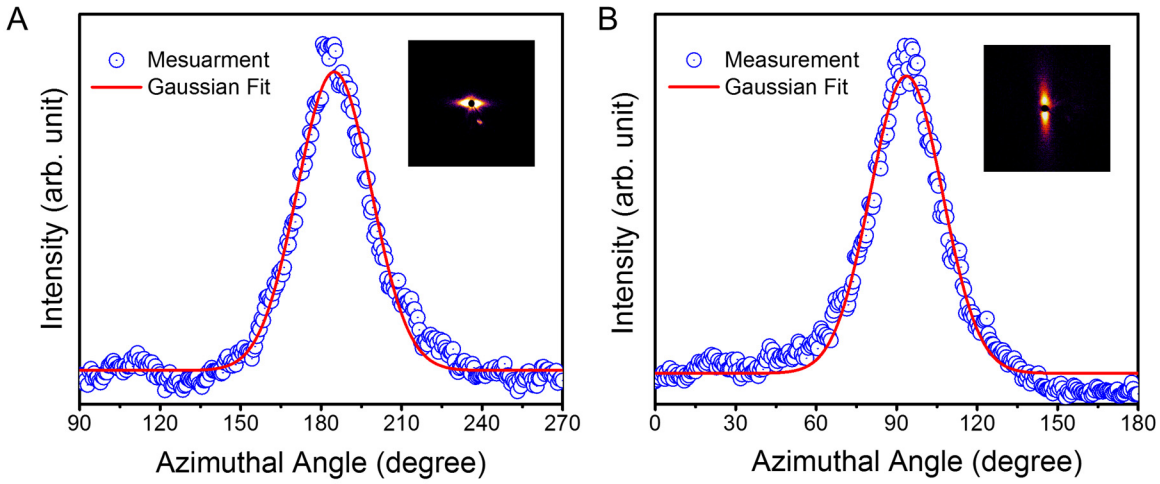

Figure S6. Azimuthal dependence of small-angle X-ray scattering (SAXS) intensity as measured by a 2D detector with the accessible range of scattering vector q of 0.015−0.21 A^{-1} and fitted by Gaussian functions. Insets are the 2D SAXS patterns. (A) Vertically aligned GO nanosheets. (B) Planarly aligned GO nanosheets. The full-widths at half maximum (FWHM) for the Vertical-GO and the Planar-GO films were 32.4° and 31.7°, respectively, which yield almost identical orientational distribution coefficients ($S_{Vertical}$ and S_{Planar} of ~0.85), indicating the GO nanosheets are well-aligned in both films. Additionally, these S values were comparable to the calculated S value for GO suspension when under the same magnetic intensity (S_{6T} = 0.85), further demonstrating that the orientation of nanosheets was well preserved after cross-linking.

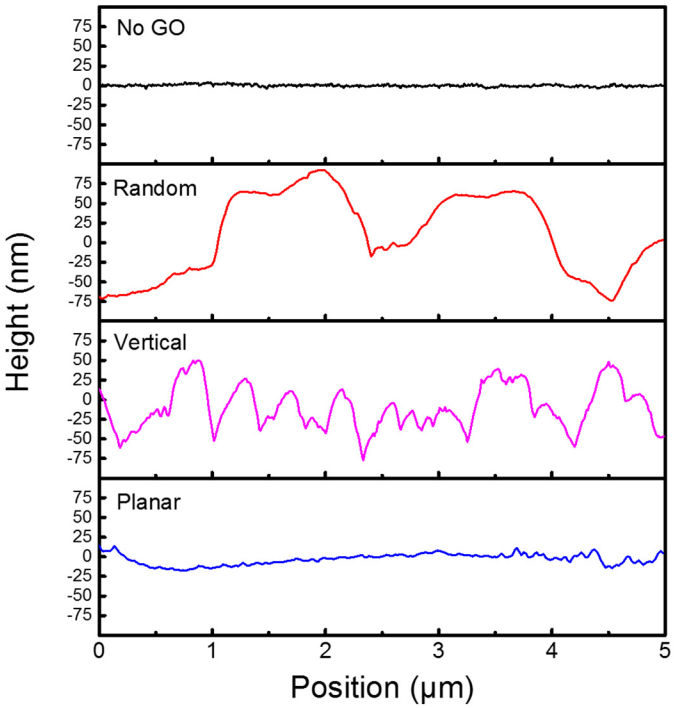

Figure S7. Representative AFM profile curves of etched GO composite films. The No-GO film (1st panel) exhibited a smooth surface. For the Random-GO (2nd panel) and Vertical-GO (3rd panel) films, the presence of GO results in a large increase in surface roughness. The surface of the Random-GO film comprised sloped ridge domains and deep valleys, which could be ascribed to the isotropic distribution of GO nanosheets. The Vertical-GO film was composed of a sharp-ridge structure on the surface, suggesting vertically aligned GO nanosheets were exposed on the surface. Compared with the Random-GO and Vertical-GO films, the Planar-GO film (4th panel) showed a much smoother surface, which is attributed to the exposure of the near-horizontal GO nanosheets on the surface.

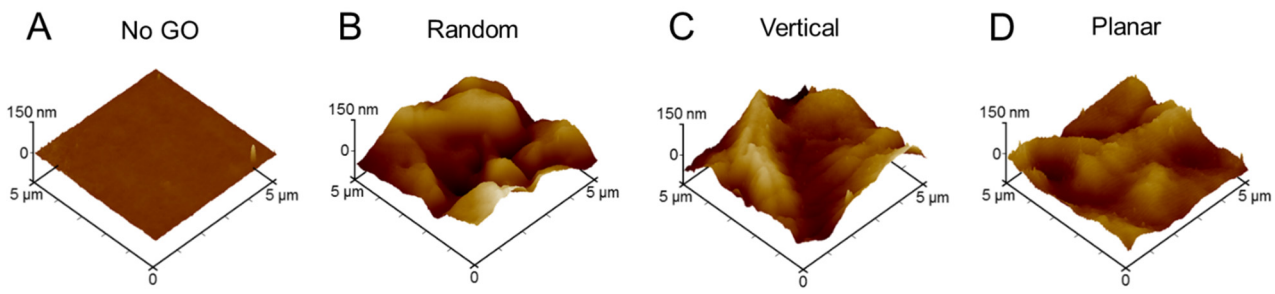

Figure S8. 3D AFM images of unetched films. The NO-GO films exhibit a smooth surface, whereas the presence of GO nanosheets increased the surface roughness of the other three films. Since the surface of the GO is covered by a top layer of poly-HEMA, all the unetched GO films showed gradually-sloped structures without obvious exposure of GO edges, in contrast with the edges clearly present on the etched samples (Figure 3). Imaging of the samples was performed in peak force tapping mode with silicon probes that had a spring constant of 0.4 N m^{-1}, resonance frequency of 70 kHz, and cantilever length of 115 ± 15 µm.

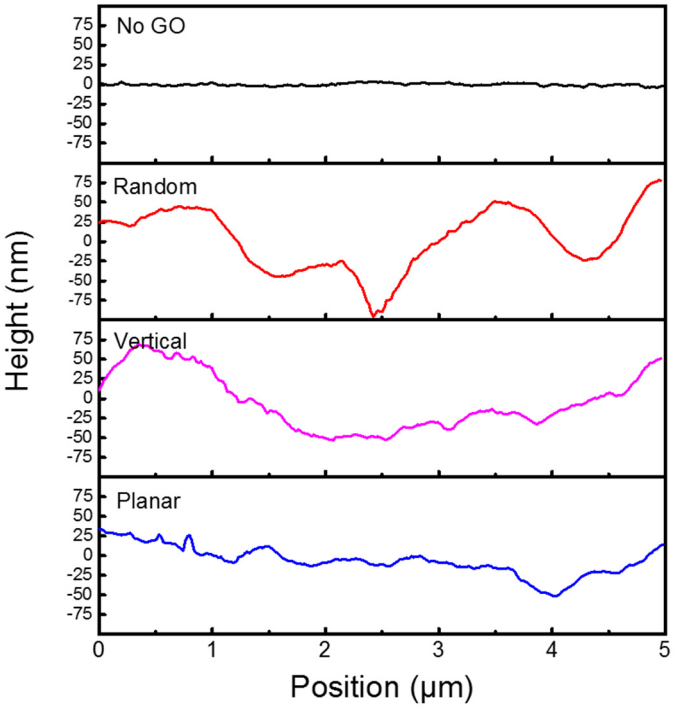

Figure S9. Representative AFM profile curves of the unetched GO composite films. The No-GO film showed a flat surface. The presence of GO results in increased surface roughness. However, without the etching, the Vertical-GO film (3rd panel) does not show the sharp-ridge structure observed for the respective etched sample in Figure S7 above, indicating the need for UV/O_3 etching to expose GO nanosheets on the film surface.

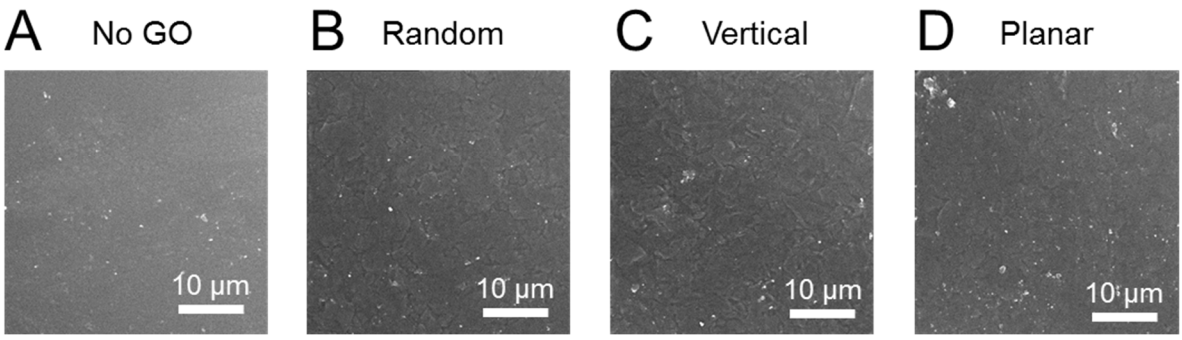

Figure S10. SEM micrographs of the unetched films. All the unetched films did not show the presence of GO edges on the surfaces, as the GO nanosheets were likely covered by a layer of poly-HEMA. The film samples were air-dried overnight, sputter-coated with an 8-nm-thick layer of iridium and observed using SEM with an accelerating voltage of 5 kV.

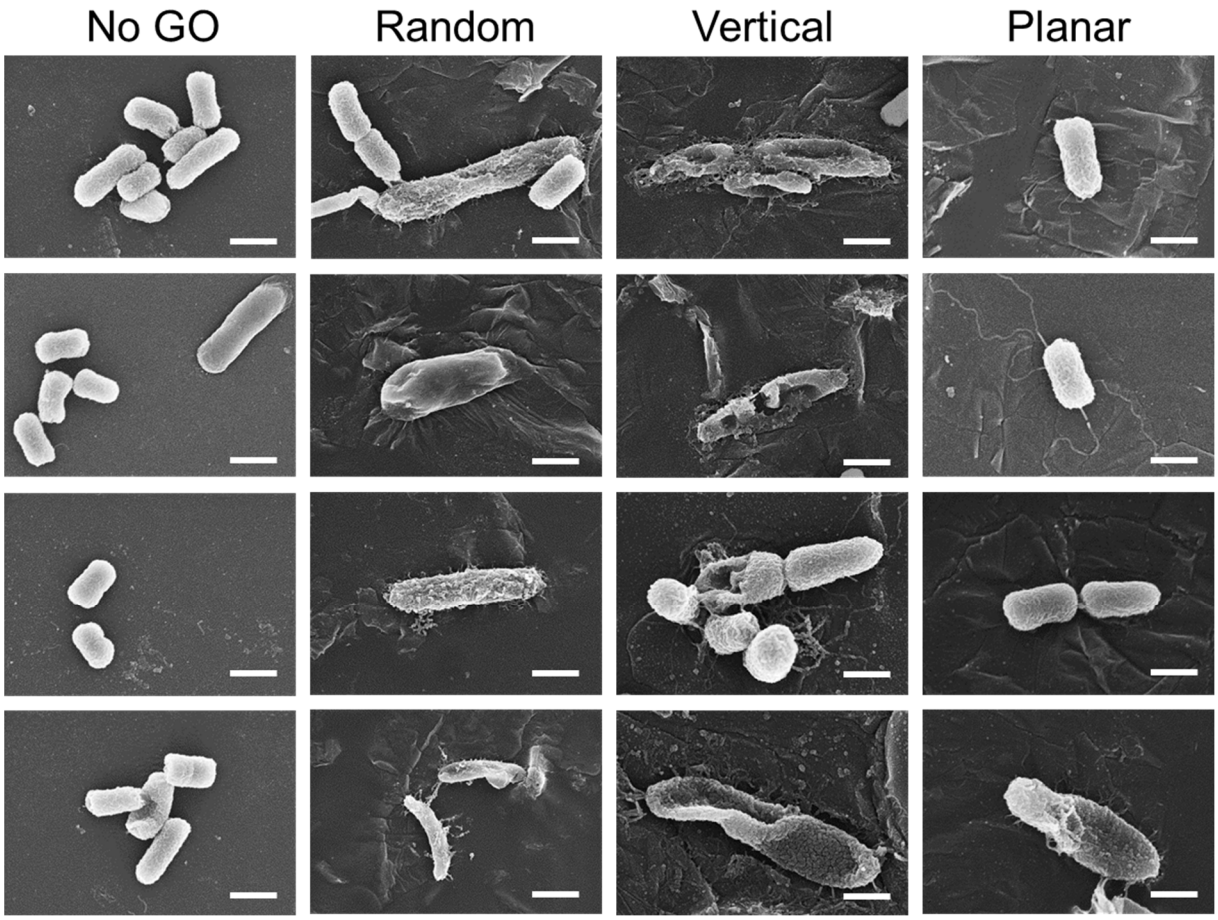

Figure S11. Representative SEM micrographs of *E. coli* cells on etched GO composite films. After 3-h exposure, the films were washed with saline solution and sequentially immersed in Karnovsky's fixative, water/ethanol mixture, and ethanol/freon to retain the morphology of the cells. The dry film samples were subsequently sputter-coated with 8-nm iridium and observed by SEM with an accelerating voltage of 5 kV. The bacteria on the No-GO film showed intact cell morphology, indicating no cytotoxicity of the pure polymer. Among the three GO composite films, the cells on the Planar-GO film largely retained their morphological integrity, whereas the cells on the Random-GO and Vertical-GO Films became flattened and wrinkled, suggesting the loss of viability. Additionally, the dead cells on the Vertical-GO films showed damage to the cell membrane, as indicated by the observable leakage of cytoplasmic matrix on the surface. The scale bar is 1 μm.

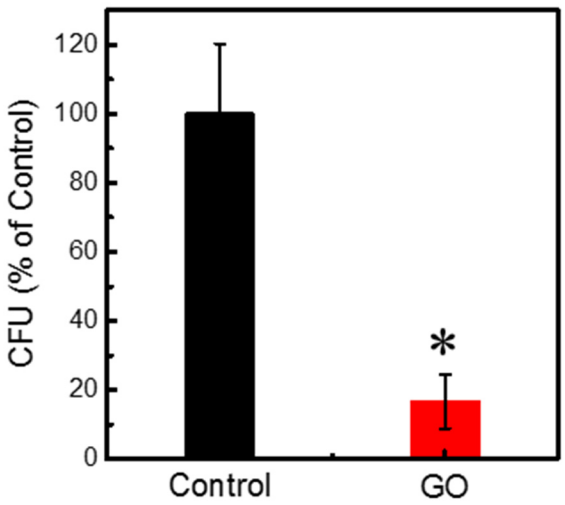

Figure S12. Antibacterial properties of GO nanosheets in suspension. Relative number of viable *E. coli* cells were determined by CFU agar plate counting and normalized to the results of the control sample. *E. coli* suspension (10^7 cfu·mL^{-1}) was exposed to GO nanosheets (200 μg·mL^{-1}) for 3 h at room temperature under constant agitation. At the end of the exposure period, the bacterial suspension was bath-sonicated for 10 min to break aggregates. The bacterial suspensions were immediately cultured on LB agar media and incubated overnight at 37 °C for CFU enumeration. The control sample underwent the identical procedure without adding GO nanosheets. Values marked with one asterisk (*) are significantly different from the value of "Control" sample (Student's *t* test, $n = 3$, $P < 0.05$). It should be noted that marginal carryover of GO nanosheets onto the LB agar media may have extended the overall exposure time of *E. coli* to GO, thereby contributing to the observed toxicity.

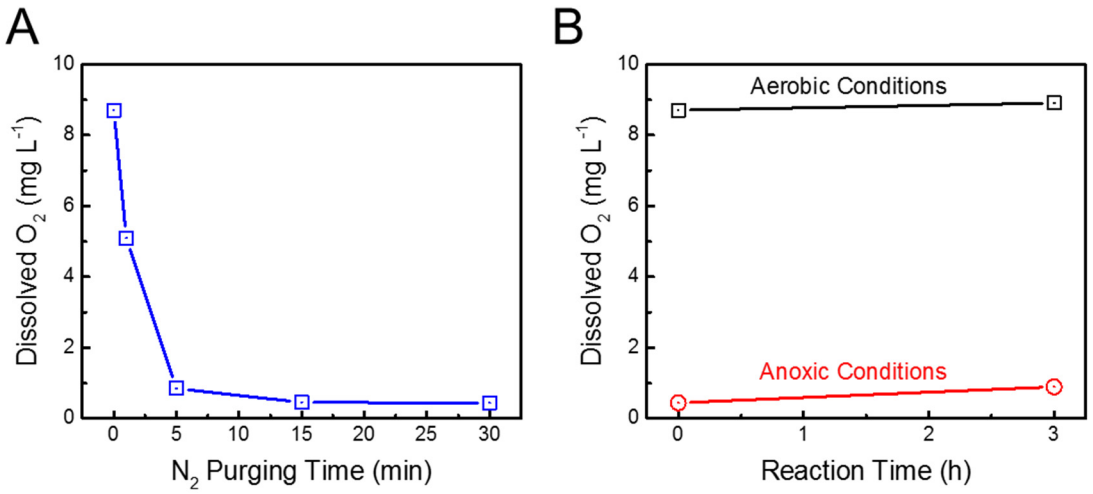

Figure S13. Concentration of dissolved oxygen (DO) in solutions used for the glutathione oxidation assay at ambient temperature (22 °C). (A) Concentration of DO after purging N_2 with different time. The DO concentration sharply decreased from 8.7 mg·L^{-1} to 0.4 mg·L^{-1} in the first 15 min. (B) DO concentration of solutions in sealed vials over the course of the 3-h reaction. The reaction vials were tightly sealed with rubber caps, and the DO was near-constant for both aerobic and anoxic conditions.

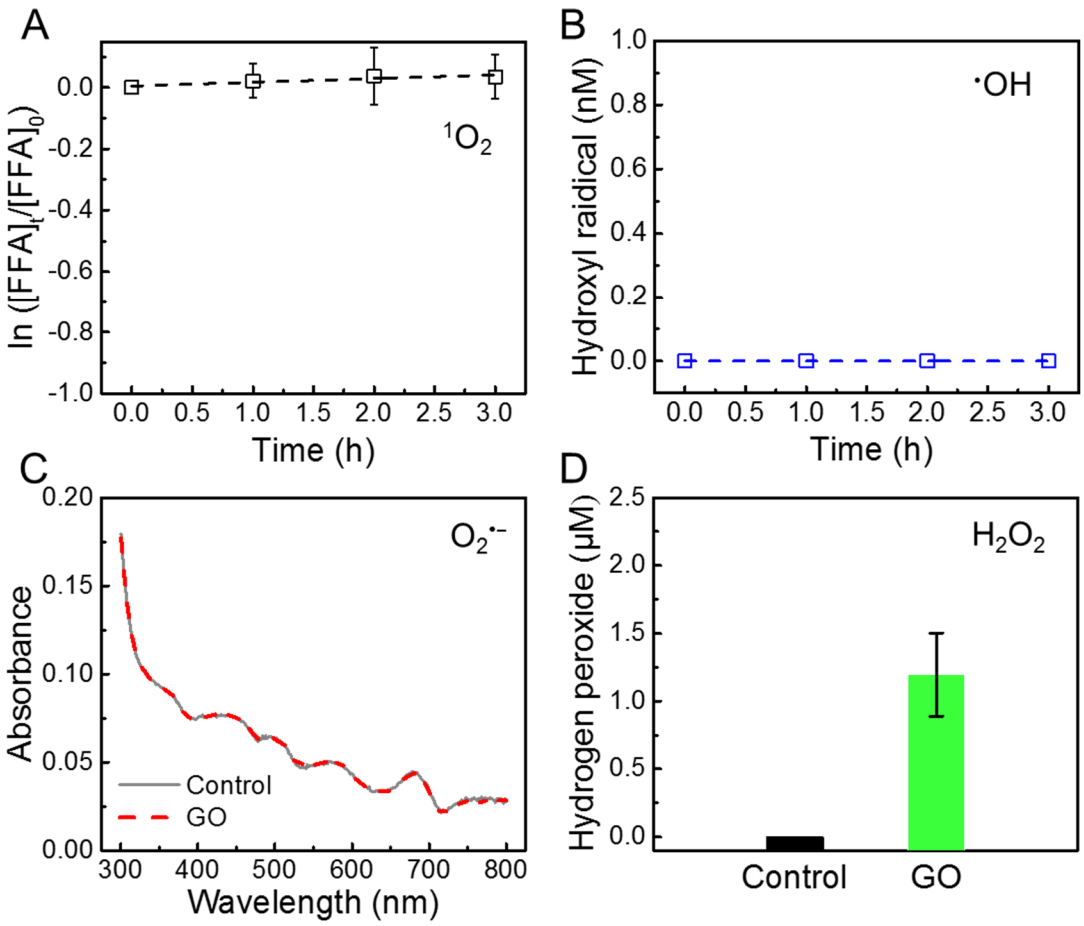

Figure S14. Detection of the four most common reactive oxygen species in a mixture of GO nanosheets and bacteria. Cell suspension (10^7 cfu·mL^{-1} *E. coli*) was exposed to 200 μg·mL^{-1} GO with individual ROS probe. The experiments were conducted in the dark at room temperature under constant agitation for 3 h. (A) Singlet oxygen ($^1O_2$) generation indicated by decay of furfuryl alcohol (FFA, initial concentration of 50 μM). (B) Cumulative hydroxyl radical (•OH) generation over time indicated by the formation of hydroxyterephthalate (hTPA). (C) Superoxide radical anion ($O_2^{\bullet-}$) generation indicated by the reduction of 2,3-Bis-(2-methoxy-4-nitro-5-sulfophenyl)-2H-tetrazolium-5-carboxanilide (XTT, initial concentration of 100 μM). (D) H_2O_2 concentration measured by the Amplex Red assay. The results show that there was no detectable generation of $^1O_2$, •OH, or $O_2^{\bullet-}$ and minor formation (~1.19 μM) of H_2O_2 with the presence of GO in *E. coli* suspension.

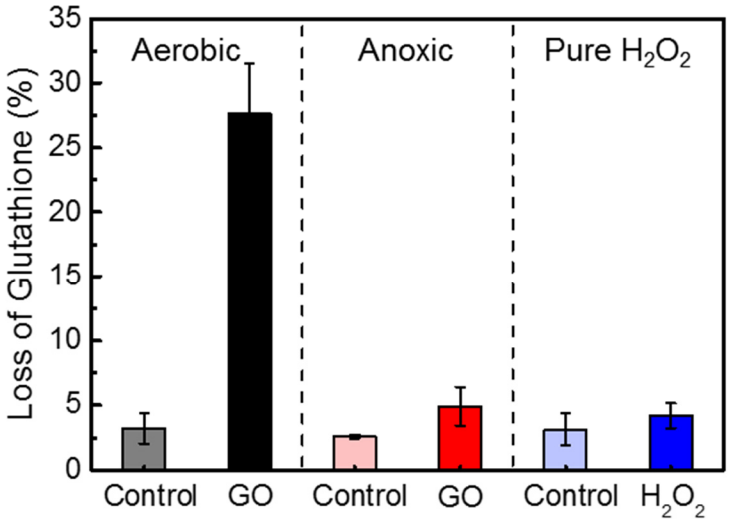

Figure S15. Comparison of *in vitro* glutathione oxidation in GO suspension and in pure H_2O_2 solution. Glutathione (0.4 mM) was exposed to 0 (control) or 200 μg·mL^{-1} GO in bicarbonate buffer (50 mM, pH 8.6) at room temperature for 3 h. For the aerobic condition (left panel), the solution was prepared without any treatment and the dissolved oxygen was ~8.7 mg·L^{-1}. For the anoxic condition (middle panel), the solution was purged with nitrogen gas for 30 min to decrease the dissolved oxygen to ~0.4 mg·L^{-1}. For the pure H_2O_2 exposure (right panel), glutathione was exposed to 2 μM of H_2O_2 under an aerobic condition. The marginal oxidation of glutathione under H_2O_2 exposure indicated that reactive oxygen species generation was not a major cause for the oxidation of glutathione with the presence of GO nanosheets under the aerobic condition.

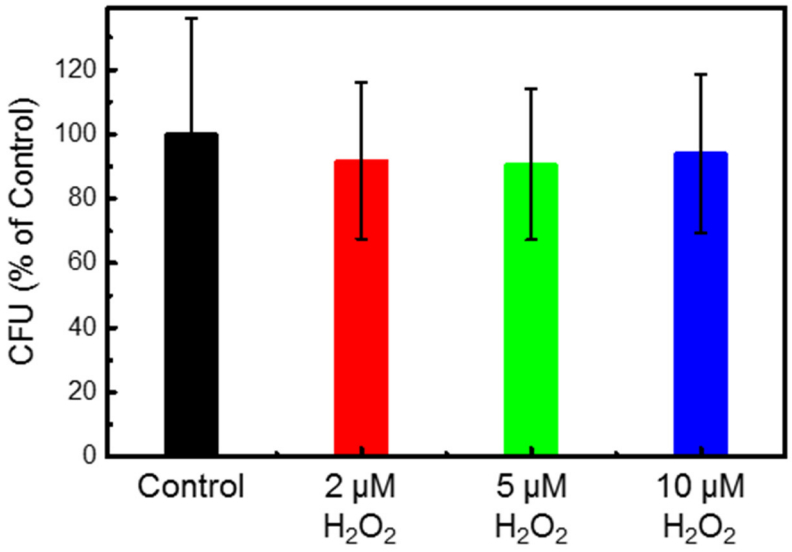

Figure S16. Relative number of viable *E. coli* cells after 3 h of contact with different concentrations of H_2O_2, determined by CFU agar plate counting and normalized to the results of the control sample. The H_2O_2 concentration (2–10 μM) used here was close to the H_2O_2 concentration (~1.76 μM) detected in 200 μg·L^{-1} GO suspension. The CFU values of the H_2O_2 exposure are not significantly different from that of the control sample (Student's *t* test, $n = 3$, $P < 0.05$), indicating limited toxicity for *E. coli* upon exposure to H_2O_2 over the concentration range of interest.

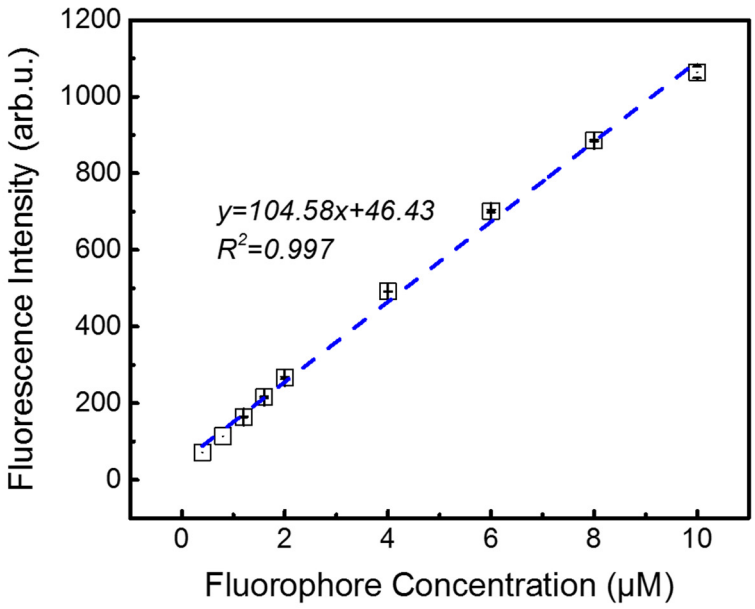

Figure S17. Standard curve of fluorophore concentration and total fluorescence. Carboxyfluorescein dye was dissolved in 50 mM MOPS buffer (pH 7.5) and 90 mM NaCl. Fluorescence intensity was monitored using a spectrofluorometer at excitation and emission wavelengths of 485 nm and 528 nm, respectively.

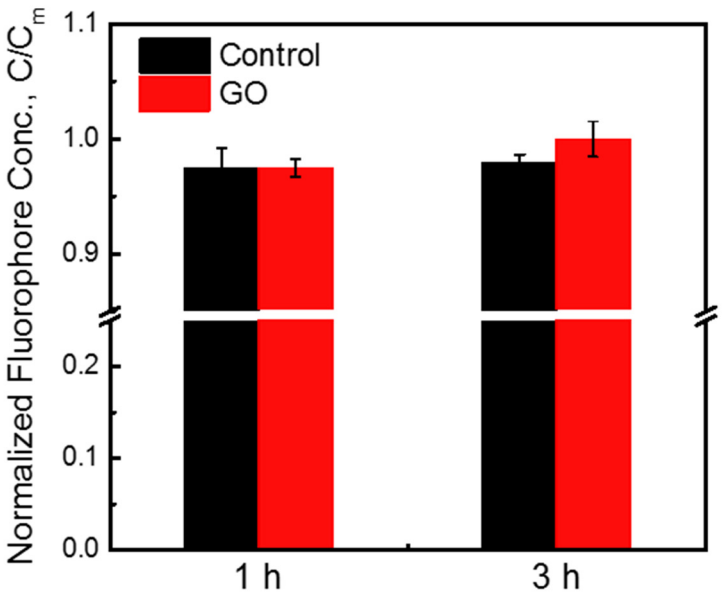

Figure S18. Adsorption of fluorophore on GO in vesicle suspension. Solutions containing 0.1 mg·mL^{-1} lipid vesicles and 10 μM extravesicular carboxyfluorescein dye were exposed to GO (40 μg·mL^{-1}) in 50 mM MOPS buffer (pH 7.5) and 90 mM NaCl at ambient temperature. A blank solution containing lipid vesicles and extravesicular dye mixture without GO nanosheets was used as a control. Fluorescence was monitored to determine the normalized fluorophore concentration (C/C_m). No decrease of fluorophore concentration in the extravesicular solution was detected after 1-h or 3-h exposure, suggesting that GO has negligible adsorption of the fluorophore in the vesicle suspension.